Investigation on the Dynamic Behavior of the Fiber in the Vortex Spinning Nozzle and Effects of Some Nozzle Structure Parameters

Zeguang Pei, Chongwen Yu

Donghua University, Shanghai, CHINA

Correspondence to:
Chongwen Yu email: yucw@dhu.edu.cn

ABSTRACT

Vortex spinning, which adopts high speed airflow to insert twist into the yarn, is one of the most promising technological innovations in the textile industry. In vortex spinning, the dynamic behavior of the fiber inside the nozzle, which involves fiber-airflow interaction and fiber-wall contact, plays an important role in the twist insertion process. This paper investigates the airflow characteristics and the fiber dynamic behavior inside the vortex spinning nozzle via a two-dimensional numerical model with the fiber-airflow interaction and fiber-wall contact included. The fiber is assumed to be isotropic, elastic material. The airflow inside the nozzle is assumed to be turbulent, viscous and incompressible. The numerical results show that two vortices with momentarily changed sizes are created upstream of the jet orifice outlets. The imbalance of the pressure around the fiber causes the fiber to move and deform. The trailing end of the fiber rotates with wave shape within the nozzle chamber for several periods to insert twist into the yarn. Based on the model, the effects of three nozzle structure parameters – the jet orifice angle, jet orifice diameter, distance between the nozzle inlet and the hollow spindle, on the dynamic behavior of the fiber, and in turn, the yarn structure and tensile property are investigated. The results show that the appropriate jet orifice angle for obtaining the best yarn tenacity is 70°. The optimal jet orifice diameter is 0.4 mm. The spun yarn has the highest tenacity when the distance between the nozzle inlet and the hollow spindle is 14 mm.

INTRODUCTION

In the twist insertion process of spinning a staple yarn, a strand of fibers is held on one end while the strand length is made to rotate on its axis. The rotation of the strand causes the fibers to adopt helical forms and increase the number of turns of twist. With the insertion of the twist, the fibers are packed together toform a continuous yarn with special structure and properties. The conventional ring spinning, which uses revolutionary mechanical part to insert twist into the yarn, is currently the most widely used spinning technique. Although ring spinning has the widest spinnable count range, its disadvantages such as low production speed, long processing procedure, and high energy consumption, have limited its productivity and process economy. Comparatively, the vortex spinning technique utilizes high speed airflow to insert twist into the yarn. This greatly increases the rotational speed of the fiber strand, which can be as high as 200, 000 turns/min. This technique not only increases the production speed and shortens the processing procedure, but also lowers the cost and energy consumption involved in the yarn production [1]. In the global background of energy shortage and manpower cost rising, the vortex spinning technique is one of the most promising technological innovations in the textile industry. In the vortex spinning system, as shown in *Figure 1*, the spinning part is composed of an air-jet nozzle and a hollow spindle with a yarn passage through it. The fibers coming from the front rollers are held together and twisted with the action of the high speed airflow inside the nozzle. Fibers that whirl around the hollow spindle tip attach to the core fibers by wrapping onto them and yarn with a similarly real-twisted structure is formed. The formed yarn is then delivered out of the nozzle through the yarn passage of the hollow spindle with the drag of the delivery rollers and fed to the winding part. The most featuring characteristic of the vortex spinning is that it is capable of spinning 100% cotton fibers at very high speed (450m/min) and the produced yarn has a structure much similar to the ring spun yarn [2].

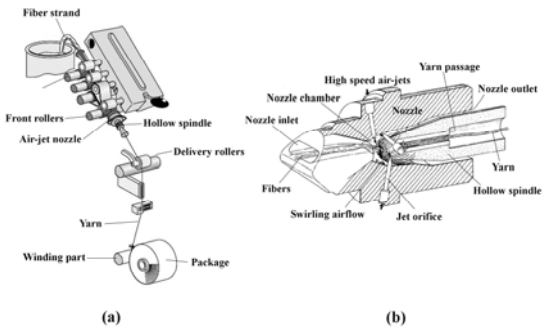

FIGURE 1. Vortex spinning system: (a) spinning unit; (b) nozzle structure [3].

Some researchers have pointed out that the dynamic behavior of the fiber in the airflow field inside the nozzle plays an important role in the twist insertion process of vortex spinning [4-5]. The research on the dynamic behavior of the fiber inside the nozzle of vortex spinning has been taken stage by stage. Since the internal airflow field inside the nozzle is very complex, there is a scarcity of publications on investigating the dynamic behavior of the fiber experimentally. With the development of computer-aided technology, computational fluid dynamics (CFD) has provided an important means of predicting the flow field under a wide range of design and operating conditions. In recent years, computational fluid dynamics approaches have been used to investigate the airflow characteristics in the vortex spinning nozzle. Pei *et al*. investigated the airflow field inside the vortex spinning nozzle by a three-dimensional CFD model [6]. Based on the characteristics of the airflow field inside the nozzle of the vortex spinning, the possible dynamic behavior of the fibers in the nozzle was discussed. However, these studies only obtained the data of the single phase – airflow without obtaining the direct data of the dynamic behavior of the fibers while the actual spinning process falls into the two-phase flow field. When a fiber is moving in the airflow, interaction between the fiber and the airflow takes place [4, 7, 8]. With the action of the airflow, the fiber which is highly flexible and possesses extremely large aspect ratio yields to the tractions of the airflow. Tractions of the airflow cause the fiber to deform and move. At the same time, the flexible deformation of the fiber changes the airflow characteristics. Therefore, the dynamic behavior of the flexible fiber in the airflow inside the vortex spinning nozzle should be investigated directly. Several flexible fiber models have been constructed. Most of the researchers modeled the flexible fiber as a chain of spherical beads linked to each other by connectors [9-12]. External forces from the flow field are only applied onto the beads. The connector between the beads only serves to transmit the internal forces and maintain the fiber configuration. The connectors do not interact with the flow. The bead-chained fiber models are too simple to describe either the exact forces acting on a fiber or the physical properties of a fiber. In addition, the interactions between the fiber and the airflow were not taken into consideration in these studies. Besides, contact and friction take place between the fiber and the nozzle wall, which influences the dynamic behavior of the fiber [13]. Due to the complexity of the mechanical problems involved, the fluid-structure interaction (FSI) model with contact between the fiber and the nozzle wall for the dynamic behavior of the fiber in the airflow inside the vortex spinning nozzle has not been reported up till now.

The vortex spun yarn has a wrapped structure with a core of twistless, parallel fibers held together by helical surface wrapper fibers. The feature of the yarn structure mainly depends on the configuration of the wrapper fibers [14]. The “process-fiber dynamic behavior–structure-property” relationship model for the vortex spun yarns is widely accepted by the researchers in this study field. “Process” means all kinds of parameters, including process parameters, nozzle structure parameters, and fiber parameters. The variation of parameter values influences the airflow characteristics inside the nozzle and the dynamic behavior of the fiber, and in turn, the yarn structure and yarn properties. To date, some works have studied the “process-structure-property” relationship in vortex spinning. Most of these works were experimental. Ortlek *et al.* studied the effect of the hollow spindle diameter and hollow spindle working period on the properties of 100% viscose vortex yarns [13]. Ortlek *et al.* also examined the influence of delivery speed, nozzle pressure, and yarn count on the properties of vortex yarn [15]. Basal *et al.* investigated a number of parameters, including the jet orifice angle, nozzle pressure, hollow spindle diameter, yarn delivery speed, and distance between the front roller and the hollow spindle, on the structure and properties of the cotton vortex yarn [16]. Numerical studies are also reported on investigating the effect of parameters on vortex spun yarn

properties. Guo *et al.* constructed a two-dimensional model and simulated the airflow pattern inside the vortex spinning nozzle to study the effect of the cone angle of the hollow spindle on the yarn properties [17]. Pei *et al.* performed three-dimensional simulations on the airflow field inside the vortex spinning nozzle. Based on the simulation results, the influences of the nozzle pressure, jet orifice angle, twisting surface angle, and the distance between the nozzle inlet and the hollow spindle on the tensile property of the vortex yarn were discussed [18]. As can be seen from the literature review above, there is a great necessity to investigate the fiber-airflow interaction and the dynamic behavior of the fiber in the vortex spinning nozzle to connect the roles played by various process parameters with the yarn structure and properties.

In this paper, a two-dimensional model for the dynamic behavior of a single cotton fiber in the airflow inside the vortex spinning nozzle is introduced. The fiber-airflow interaction and the contact between the fiber and the nozzle wall during the fiber motional process are incorporated. Based on the model, the effects of three nozzle structure parameters – the jet orifice angle, jet orifice diameter, distance between the nozzle inlet and the hollow spindle, on the dynamic behavior of the fiber, in turn, the yarn structure and tensile property are discussed. Seven cases with different parameter settings, as shown in *Table I*, are adopted in the simulation. Nozzle structure is changed for different cases according to the corresponding parameter values. The rest of the parameter values are kept unchanged. The fluid-structure interaction model combined with the fiber-wall contact has not been reported in the research on the dynamic behavior of the fiber in the vortex spinning nozzle. The goal of this work is to extend the current computational simulation methodology for the dynamic behavior of the fiber in the vortex spinning nozzle to a new stage with fiber-airflow interaction being solved and to provide an efficient way of investigating the roles played by various process parameters on the yarn properties. The methodology provided in this work can be extended to the solution of the mechanical problems in other textile processes involving fluid-structure interactions.

Table I. Parameter values for the computation cases

Case	Jet orifice angle (degree)	Jet orifice diameter (mm)	Distance between nozzle inlet and spindle (mm)
A	60	0.4	14
B	70	0.4	14
C	80	0.4	14
D	70	0.35	14
E	70	0.45	14
F	70	0.4	13
G	70	0.4	13.5

MODELING

Governing Equations of Airflow and Fiber

The airflow inside the vortex spinning nozzle is assumed to be turbulent, viscous and incompressible. The fiber undergoes free movement and large deformation momentarily when it is moving inside the nozzle. Hence, the airflow domain varies accordingly. The arbitrary Lagrangian-Eulerian (ALE) technique is adopted to deal with the variation of the airflow domain. The Navier-Stokes equation with arbitrary Lagrangian-Eulerian (ALE) description is employed as the governing equation for the airflow field:

$$\rho_a\left(\frac{\partial \boldsymbol{u}_a}{\partial t}+(\boldsymbol{u}_a-\boldsymbol{u}_m)\cdot\nabla\boldsymbol{u}_a\right)=-\nabla p_a+\mu_a\nabla^2\boldsymbol{u}_a+\boldsymbol{f}_a^B \qquad (1)$$

and the continuity equation:

$$\nabla\cdot\boldsymbol{u}_a=0 \qquad (2)$$

where $\boldsymbol{u}_a$ is the airflow velocity, $\boldsymbol{u}_m$ is the arbitrary velocity of the fluid mesh, ρ_a is the air density, p_a is the air pressure, μ_a is the dynamic viscosity of the air and $\boldsymbol{f}_a^B$ represents the body force. The air has a density ρ_a=1.225 kg·m^{-3} and a dynamic viscosity μ_a=1.7894×10^{-5} kg·m^{-1}·s^{-1}.

Due to the high Reynolds number of the airflow, the airflow inside the vortex spinning nozzle operates in the turbulent regime [6]. The standard k-ε model is employed to model the turbulence of the airflow. In the ALE coordinate system, the transportation equations for k and ε are:

$$\rho_a \frac{\partial k}{\partial t} + \rho_a (\boldsymbol{u}_a - \boldsymbol{u}_m) \cdot \nabla k = \nabla \cdot ((\mu_0 + \frac{\mu_t}{\sigma_k}) \nabla k) + 2\mu_t D^2 - \rho_a \varepsilon \quad (3)$$

$$\rho_a \frac{\partial \varepsilon}{\partial t} + \rho_a (\boldsymbol{u}_a - \boldsymbol{u}_m) \cdot \nabla \varepsilon = \nabla \cdot ((\mu_0 + \frac{\mu_t}{\sigma_\varepsilon}) \nabla \varepsilon) + \frac{\varepsilon}{k}[2c_1 \mu_t D^2 - c_2 \rho_a \varepsilon] \quad (4)$$

where k is the kinetic energy of the turbulence, ε is the dissipation rate of the turbulence, μ_0 is the laminar viscosity, $\mu_t (= \rho_a c_1 \frac{k^2}{\varepsilon})$ is the turbulence viscosity, D ($= \sqrt{\mathbf{e} \otimes \mathbf{e}}$, $\mathbf{e} = \frac{1}{2}[\nabla \boldsymbol{u}_a + (\nabla \boldsymbol{u}_a)^{\mathrm{T}}]$) is the strain tensor, c_μ, c_1, c_2, σ_k, σ_ε are model constants. The values of these model constants are

c_μ=0.09, c_1=1.44, c_2=1.92, σ_k=1.0, σ_ε=1.3.

The fiber is assumed to be isotropic, elastic material. The governing equation for the fiber undergoing motion is:

$$\rho_f \frac{\partial \boldsymbol{u}_f}{\partial t} = \nabla \cdot \boldsymbol{\sigma}_{ij} + \boldsymbol{f}_f^B \quad (5)$$

where ρ_f is the fiber density, $\boldsymbol{u}_f$ is the fiber velocity, $\boldsymbol{\sigma}_{ij}$ is the stress tensor, $\boldsymbol{f}_f^B$ is the body force of the fiber. Body forces $\boldsymbol{f}_a^B$ and $\boldsymbol{f}_f^B$ are zero and gravity forces are negligible since the fiber is almost buoyant. The cotton fiber, which is the most commonly used material of vortex spinning, is adopted in this simulation. The fiber density ρ_f=1.54×10^3 kg·m^{-3}, the Young's modulus of the fiber E=8×10^9 Pa and the poisson's ratio of the fiber v is taken as 0 in this work.

At the fiber-airflow interface, the kinematic condition (displacement compatibility)

$$\bar{\boldsymbol{d}}_f = \bar{\boldsymbol{d}}_a \quad (6)$$

and the dynamic condition (traction equilibrium)

$$\boldsymbol{n} \cdot \bar{\boldsymbol{\tau}}_f = \boldsymbol{n} \cdot \bar{\boldsymbol{\tau}}_a \quad (7)$$

should be satisfied, where $\bar{\boldsymbol{d}}_f$ and $\bar{\boldsymbol{d}}_a$ are the fiber and airflow displacements at the interface, respectively. $\bar{\boldsymbol{\tau}}_f$ and $\bar{\boldsymbol{\tau}}_a$ are the fiber and airflow stress at the interface, respectively. $\boldsymbol{n}$ denotes the vector of the normal direction of the interface.

No-slip condition is applied to the fiber-airflow interface, hence

$$\bar{\boldsymbol{u}}_a = \dot{\bar{\boldsymbol{d}}}_f \quad (8)$$

where $\bar{\boldsymbol{u}}_a$ is the airflow velocity at the fiber-airflow interface.

Contact Conditions

As mentioned in Ref [13], when the fiber is moving inside the vortex spinning nozzle, it contacts the internal wall of the hollow spindle. During the fiber motional process, it is previously unknown when and where the fiber contacts the wall. In addition, due to the flexibility and large aspect ratio of the textile fiber, different parts of the fiber may contact the wall simultaneously. Suppose N bodies (different parts of the fiber and the walls) that are in contact at time t. The dynamic equilibrium for the N bodies in the contact system at time t is given by the principle of virtual work [19]:

$$\sum_{i=1}^{N} \left\{ \int_{{}^tV} \boldsymbol{\tau} \cdot \delta \boldsymbol{\varepsilon} \, \mathrm{d}^t V \right\} = \sum_{i=1}^{N} \left\{ \int_{{}^tV} \boldsymbol{f}^{\boldsymbol{B}} \cdot \delta \boldsymbol{u} \, \mathrm{d}^t V + \int_{{}^tS_f} \boldsymbol{f}^{\boldsymbol{S}} \cdot \delta \boldsymbol{u} \, \mathrm{d}^t S \right\} + \sum_{i=1}^{N} \int_{{}^tS_c} \boldsymbol{f}^{\boldsymbol{c}} \cdot \delta \boldsymbol{u} \, d^t S \quad (9)$$

where $\boldsymbol{\tau}$ is the second Piola-Kirchhoff stress tensor, $\boldsymbol{\varepsilon}$

is the Green-Lagrange strain tensor, $\boldsymbol{f}^{B}$ is the body force, $\boldsymbol{u}$ is the displacement, ${}^{t}V$ is the volume of the ith body, ${}^{t}S_c$ is the contact area for body i, i=1,…, N,

$\boldsymbol{f}^{S}$ is the externally applied traction acting over the area ${}^{t}S_f$, $\boldsymbol{f}^{c}$ is the contact traction acting over the area ${}^{t}S_c$.

For simplification, the friction between the fiber and the wall is neglected in the present work. The normal contact conditions can be expressed as

$$g \geq 0; \lambda \geq 0; g\lambda \geq 0 \qquad (10)$$

where g is the gap function, λ is the normal contact force.

Model Geometry

Figure 2 shows the initial geometry of the computational domains of the airflow and the fiber in case B. In order to keep the computational results in a good precision, all lengths in this work are in millimeters. Masses and times are in kilograms and seconds, respectively. All the units of the rest quantities are consistent with the length, mass and time units. The computational domain of the airflow is the cavity inside the nozzle. The Cartesian coordinate system is adopted. The two-dimensional computational domains locate in the y-z plane. The center of the nozzle inlet is taken as the origin of the Cartesian coordinate system. The y-axis of the coordinate system is set superposed with the nozzle axis and points from the nozzle inlet toward the downstream. The airflows are jetted into the nozzle through the inclined jet orifices which are connected to the air compressor. The jet orifice angle is the angle between the nozzle axis and the jet orifice axis. A hollow spindle with a tapered portion in the inlet end locates slightly downstream of the jet orifices. The hollow spindle defines a passage whose inlet portion has a relative small diameter. The diameter of the passage has a sudden increase at the back end portion. The outlet of the hollow spindle is used for delivering the spun yarn out of the nozzle. A cylindrical cavity having a relatively small diameter is formed inside the nozzle wall that surrounds the tapered portion of the hollow spindle. The diameter of the back end of the cavity is slightly greater than that of the back end of the hollow spindle. The textile fiber is assumed to be a thin long cylindrical object with very large aspect ratio. In the two-dimensional simulation, the fiber with no force applied on it is taken as a rectangular continuum. In this work, the length of the fiber is 30 mm and the diameter of the fiber is 0.02 mm. At the beginning of the simulation, the entire fiber is assumed to have entered the nozzle.

The fiber domain is surrounded by the airflow domain. The longitudinal axis of the fiber is parallel to the nozzle axis and is placed at z=0.06 mm. The trailing tip of the fiber is placed at y=1 mm. The leading end of the fiber has been drawn into the hollow spindle by the fibers of the preceding portion of the fiber strand being twisted into the spun yarn [3].

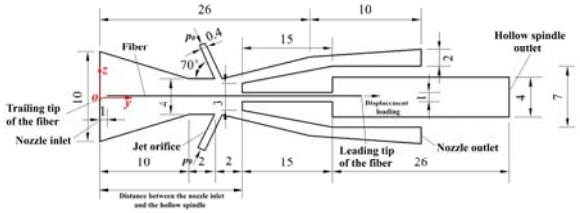

FIGURE 2. Initial geometry of the computational domains of the airflow and the fiber of case B (unit: mm).

Grid Generation

3-node triangular elements are used to discretize the entire airflow domain due to the complexity of the computational domain. Finer element edge lengths are adopted through the jet orifices, the cavity surrounding the tapered portion of the hollow spindle and near the fiber-airflow interface. To verify the grid independence, numerical simulations of the fiber motions are performed on four different meshes with 4741, 5440, 6975 and 8674 triangular elements in the fluid. Accordingly, the fiber domain is discretized into 1×200 (1 element across the radial direction of the fiber and 200 elements along the length), 1×250, 1×300 and 1×400 9-node quadrilateral elements with equal sizes, respectively. The two sets of grids conform at the interface. Very good agreements between the two finer sets of the mesh solutions of the fiber motional characteristics are obtained. The differences in both the simulated rotational amplitude and period are less than 5%. Therefore, a grid with 6975 triangular elements in the fluid domain and 1×300 9-node quadrilateral elements with equal sizes in the fiber domain are adopted for the simulation.

Figure 3 presents the grid generated for the model of Case B.

Boundary Conditions and Loadings

Figure 3(a) shows the boundary conditions for the model of Case B. Fluid-structure interface and no-slip boundary conditions are applied at the fiber-airflow interface. No-slip boundary conditions are also applied to all the rigid walls of the nozzle and the hollow spindle. Prescribed velocity loadings of 202000 mm/s (202 m/s) are applied at the inlets of the jet orifices and the velocity loadings are perpendicular to the axes of the jet orifices. Distributed normal-traction loadings equal to the atmospheric pressure (101.325 kg·mm^{-1}·s^{-2} =1.01325 $\times 10^5$ Pa) are applied to all the open boundaries of the airflow domain. Prescribed displacement loading of 21 mm in the positive y direction is applied at the leading tip of the fiber to represent the motion of the leading end of the fiber driven by the drag from the fibers of the preceding portion of the fiber strand being twisted into the spun yarn [3].

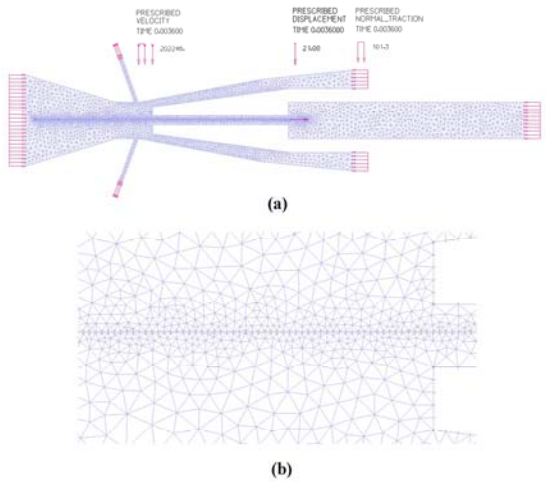

FIGURE 3. (a) Grid and boundary conditions for the model; (b) A close-up view of the grid for the fiber.

NUMERICAL METHODS

The fully coupled fluid-structure interaction model of the dynamic behavior of the fiber in the airflow inside the vortex spinning nozzle is solved using the finite element package ADINA. Before the fiber starts to move, the flow inside the nozzle is assumed to be in the fully developed steady state. The steady solution is taken as the initial condition for the transient computation of the fiber motion. To simulate the fully developed steady flow condition, the fiber is initially fixed at its initial position and is assumed to be rigid by applying no-slip wall condition to the fiber-airflow interface. The following initial conditions for the computation of the steady solution are specified throughout the airflow domain:

$$v_{0y} = 0,\ v_{0z} = 0,\ p_0 = 101.325\ \text{kg}\cdot\text{mm}^{-1}\cdot\text{s}^{-2} \qquad (11)$$

where v_{0y} is the y component of the initial airflow velocity, v_{0z} is the z component of the initial airflow velocity, p_0 is the initial airflow pressure.

Since the computation of the steady solution is a nonlinear problem, if the full loads applied at the jet orifice inlets are applied in one time step, the solution is difficult to reach convergence. Hence, the velocity loading is gradually increased from zero to the prescribed value over 10^5 time steps. A time step size of 10^{-5} s is used in the computation. The velocity loading is linearly applied. After the velocity loading reaches its prescribed value, another 10^3 time steps of computation is continued to assure the obtaining of the steady solution of the airflow field. Then the actual physical properties of the fiber, such as the Young's modulus and density, together with the actual fluid-structure interaction interface are resumed. The fiber is released with an initial velocity v_{0y}=350 m/min which is equal to the yarn delivery speed to simulate the transient motion of the fiber in the nozzle. The time step size of the transient computation is also set to be 10^{-5} s. 360 time steps are taken for the transient computation. Direct computing method is used for the FSI solution and a maximum number of 100 fluid-structure iteration is adopted. Newmark method is employed for the nonlinear dynamic analysis of the fiber motion. The FSI model is solved using the Newton-Raphson method. The relative tolerance for all degrees of freedom is set to 0.001. Since the fiber undergoes large deformation and free movement when it is moving in the nozzle, the mesh adaptivity procedure of ADINA is adopted. The mesh of the fluid domain is updated at each time step according to the configuration of the fiber obtained at the previous time step and the deformation of the mesh is checked. If unacceptable mesh deformation takes place and the mesh quality goes worse, a new mesh which may have no correspondence with the old mesh is generated for the fluid domain. Then the flow field is projected from the old mesh to the new mesh. The details of the mesh adaptivity procedure are given by Bathe and Zhang [20].

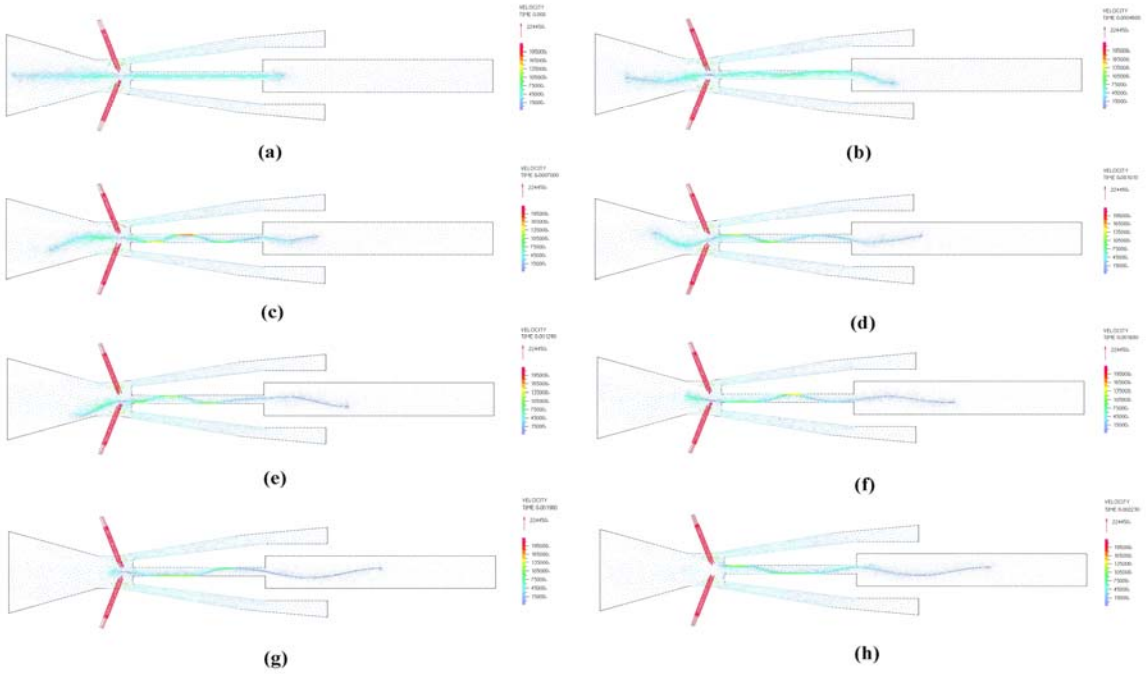

FIGURE 4. Velocity vectors (mm/s) of the airflow at different times: (a) t=0 s; (b) t=0.00046 s; (c) t=0.0007 s; (d) t=0.00101 s; (e) t=0.00129 s; (f) t=0.0016 s; (g) t=0.0019 s; (h) t=0.00232 s.

The two-dimensional contact surfaces for the wall of the small-diameter portion of the passage of the hollow spindle are defined and set to be rigid. The surfaces of the two-dimensional fiber are also set to be the contact surfaces. Two contact pairs each consisting of a contact surface on the fiber and that for the wall at the same side of the contact surface on the fiber are defined. The contact surfaces for the wall are selected to be the target surfaces and the contact surfaces on the fiber are selected to be the contactor surfaces. An element edge length of 0.05 mm is used to discretize the contact surfaces for the wall and a number of 2 nodes per segment is adopted. The constraint function method is used to enforce thecontact conditions expressed by Eq. (10).

RESULTS AND DISCUSSION

Airflow Characteristics in the Vortex Spinning Nozzle

Figure 4 shows some snapshots of the velocity vectors of the airflow in the vortex spinning nozzle of case B. *Figure 5* shows the deformed mesh of the model at t=0.00064 s. At the start of the transient computation, the airflow reaches a fully developed state *Figure 4(a*). Air-jets are ejected into the nozzle chamber through the jet orifices at a speed higher than 200 m/s. The air-jets flow toward the fiber portion slightly upstream of the hollow spindle inlet. The air-jet velocities decrease to below 90 m/s rapidly after they enter the nozzle chamber. Most of the air currents are generated in the cavity between the hollow spindle and the nozzle wall. Since the hollow spindle inlet locates downstream of the jet orifice outlets, some air currents flow into the hollow spindle close to the fiber. The rest of the air currents flow upstream toward the nozzle inlet, creating reverse flows. This is in accordant to our previous research results [6]. It also can be seen that some airflows enter the nozzle inlet from the outside and flow inside close to the nozzle wall. After the actual physical properties are resumed for the fiber, the fiber begins to move downstream with wave shape. The airflow characteristics change with the transient motion of the fiber. At t=0.00046 s *Figure 4(b)*, two vortices are created upstream of the jet orifice outlets with a vortex located at either side of the fiber. The sizes of the two vortices change momentarily. The vortex located at the opposite side to the vibration direction of the fiber is enlarged. The one located at the side in the vibration direction of the fiber is compressed. At t=0.0007 s *Figure 4(c)*, the vortex on the side in the vibration direction of the fiber is

compressed so much that it breaks into two vortices, in which a small vortex locates just upstream of the jet orifice outlet and a large vortex locates upstream of the small one. With the fiber moving downstream into the hollow spindle, the large vortex gradually sheds from the trailing end of the fiber. After the trailing tip of the fiber passes the jet orifices *Figure 4(h)*, a small vortex and a large vortex still exist in the nozzle chamber. *Figure 6* illustrates the pressure contours of the airflow at different times. It can be seen from the figure that the air pressure decreases as the air-jets flow through the jet orifice. At the outlet of the jet orifice, the air pressure reaches its minimum value. A high pressure region exists near the entrance of the hollow spindle. From this region outward, there are progressive concentric layers of decreasing pressures. It also can be seen that the pressure around the fiber is not symmetrically distributed. The region where the vortex exists is the low-pressure region. This imbalance of the pressure distribution causes the fiber to deform and the fiber vibrates to the side with lower pressures.

Dynamic Behavior of the Fiber

Figure 7 shows some snapshots of the dynamic behavior of the fiber in case B. It can be seen that the fiber shows bending deformations and vibrates with wave shape. The fiber moves downstream from its initial position and gradually enters the hollow spindle entirely. The portion of the fiber that has entered the hollow spindle contacts the internal wall of the hollow spindle frequently at different locations. Since the leading end of the fiber is gripped by thefibers of the preceding portion of the fiber strand being twisted into the spun yarn, the motional characteristics of the trailing end of the fiber are decisive to the twist insertion process. The trailing end of the fiber shows up-and-down vibrations. At the beginning, the trailing end of the fiber starts to rotate toward the nozzle wall and gradually splays out. When the trailing tip of the fiber reaches the outermost point, as shown in *Figure 7(a)*, the trailing

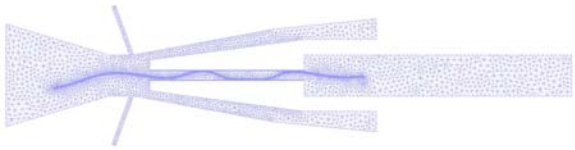

FIGURE 5. Deformed mesh of the model at t=0.00064.

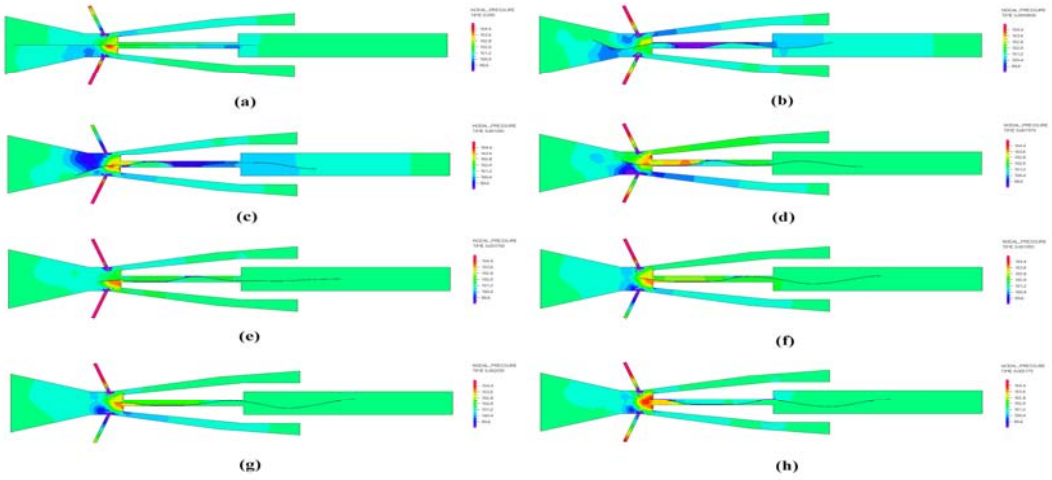

FIGURE 6. Pressure contours (kg·mm^{-1}·s^{-2}) of the airflow at different times: (a) t=0 s; (b) t=0.00096 s; (c) t=0.00126 s; (d) t=0.00157 s; (e) t=0.00176 s; (f) t=0.00195 s; (g) t=0.00203 s; (h) t=0.00217 s.

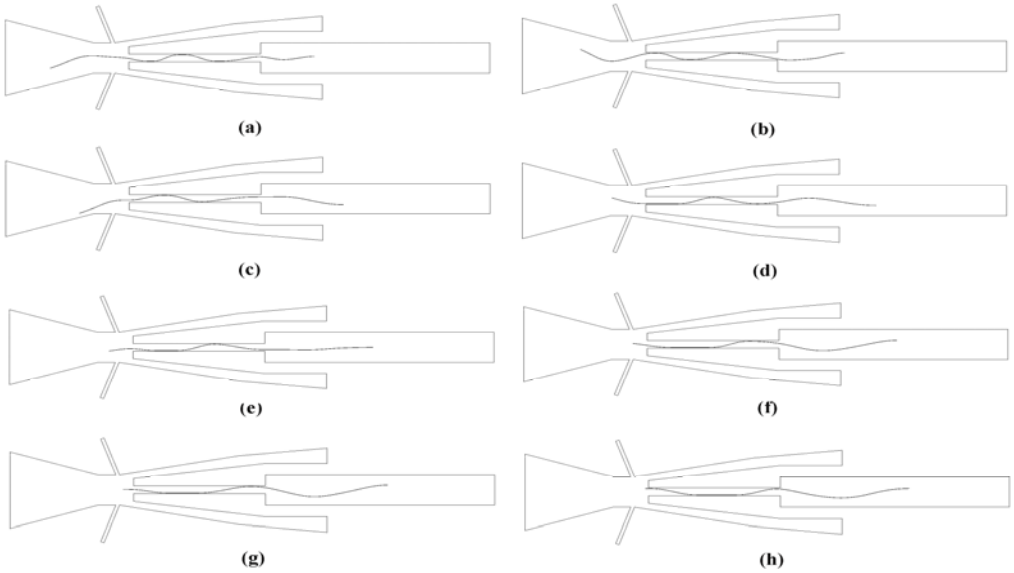

FIGURE 7. Dynamic behavior of the fiber in case B: (a) t=0.0007 s; (b) t=0.00096 s; (c) t=0.00126 s; (d) t=0.00157 s; (e) t=0.00176 s; (f) t=0.00195 s; (g) t=0.00203 s; (h) t=0.00217 s.

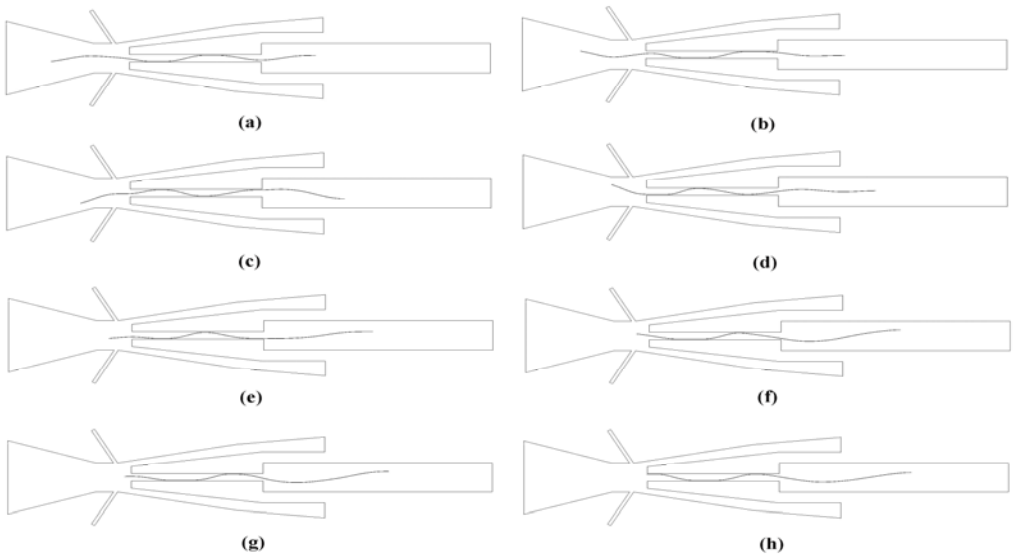

FIGURE 8. Dynamic behavior of the fiber in case A: (a) t=0.00071 s; (b) t=0.00096 s; (c) t=0.00126 s; (d) t=0.00155 s; (e) t=0.00178 s; (f) t=0.00198 s; (g) t=0.00210 s; (h) t=0.00222 s.

end of the fiber completely splays out. The splayed fibers serve as the wrapper fibers in the produced yarn. After the stage of splay, the trailing end of the fiber is in a free state. It rotates periodically for several loops within the nozzle chamber and wraps to form the spun yarn. The wrapping process or the twist insertion process takes place at this stage. After the trailing end of the fiber enters the hollow spindle entirely, the wrapping process is finished. The formed yarn moves downstream through the hollow spindle and is delivered out of the nozzle. The higher tenacity value of the vortex spun yarn can be attributed to the higher number of wrapper fibers and twists along with tighter wrapping. The greater splay degree of the

fiber indicates a larger number of the wrapper fibers. On the other hand, the number of the rotational periods of the trailing end of the fiber denotes the number of twists inserted into the yarn, while the rotational amplitude expresses the tightness of the wrapping. The higher number of the rotational periods indicates the higher the number of twists inserted into the yarn. The greater rotational amplitude indicates the tighter wrapping. As shown in *Figure 7*, three and a half periods of the wrapping of the fiber take place in case B. The first wrapping period starts at the time when the trailing end of the fiber completely splays out and ends at the time when the trailing tip of the fiber reaches its outermost point at the same side again, as shown in *Figure 7(b-c)*. Similarly, *Figure 7(d-e) shows* the second wrapping period and *Figure 7(f-g)* shows the third. With the fiber gradually moving downstream and entering the hollow spindle, the rotational amplitude of the trailing tip of the fiber gradually decreases. During the last half of the wrapping period, as shown in *Figure 7(h)*, the trailing tip of the fiber moves from the outermost point at one side to the other side. The wrapping process is finished when the entire fiber enters the hollow spindle.

Effect of the Jet Orifice Angle

Figure 8 and *Figure 9* display the simulated results of the dynamic behavior of the fiber in the cases of the jet orifice being 60° (Case A) and 80° (Case C). When the jet orifice angle is 60°, the motional configurations of the fiber are similar to those when the jet orifice angle is 70° (Case B). In the two cases, the fiber moves in the negative *z* direction to splay out. In contrast, in the case of the jet orifice angle being 80°, the fiber moves in the positive *z* direction to splay out. Among the three cases, the trailing end of the fiber has the lowest splay degree when the jet orifice angle is 60°. In this case, there are fewest fibers splaying out and fewest wrapper fibers for the produced yarn. During the wrapping process, three and a half wrapping periods occur before the trailing end of the fiber enters the hollow spindle entirely. This indicates three and a half twists are inserted into the yarn. During the first wrapping period, the rotational amplitude of the trailing end is the smallest among the three cases. The splay degree of the trailing end of the fiber does not increase with the increased jet orifice angle. When the jet orifice angle is 70°, the trailing end of the fiber has the greatest splay degree. In this case, most fibers splay out and most wrapper fibers are generated for the produced yarn. During the second, third and the last half wrapping period, the rotational amplitude of the trailing end of the fiber is similar to the case when the jet orifice angle is 60°. In the case when the jet orifice is 80°, three wrapping periods take place and three twists are inserted into the yarn. During the first wrapping period, although the trailing end of the fiber has the greatest rotational amplitude, the fiber collides with the nozzle wall *Figure 9(c)*. This leads to the wild and irregular wrapping of the fiber, thus leading to the decreased yarn tensile property [21]. During the second wrapping period, the trailing end of the fiber still has the greatest rotational amplitude of the three cases. During the third wrapping period, the rotational amplitude of the trailing end of the fiber is similar to that in the other two cases.

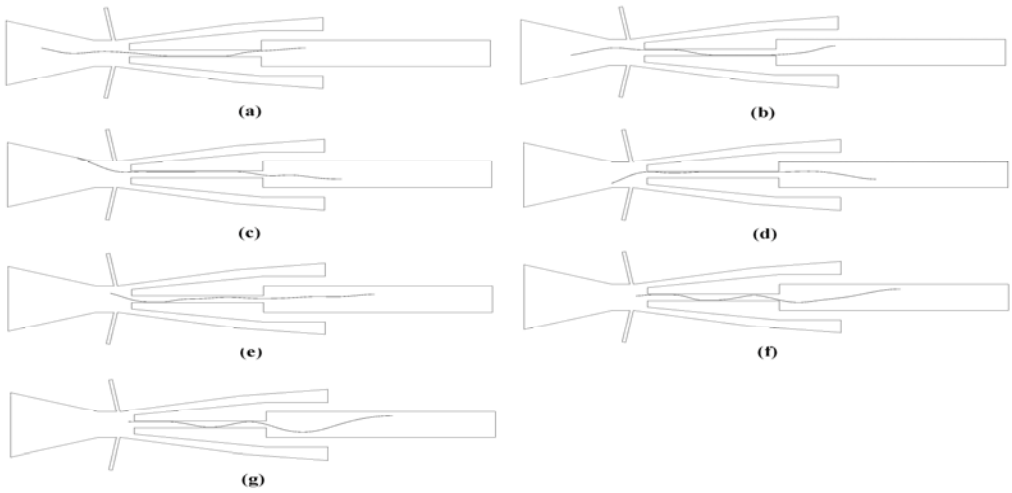

FIGURE 9. Dynamic behavior of the fiber in case C: (a) t=0.00052 s; (b) t=0.0008 s; (c) t=0.00119 s; (d) t=0.00154 s; (e) t=0.00182 s; (f) t=0.00201 s; (g) t=0.00212 s.

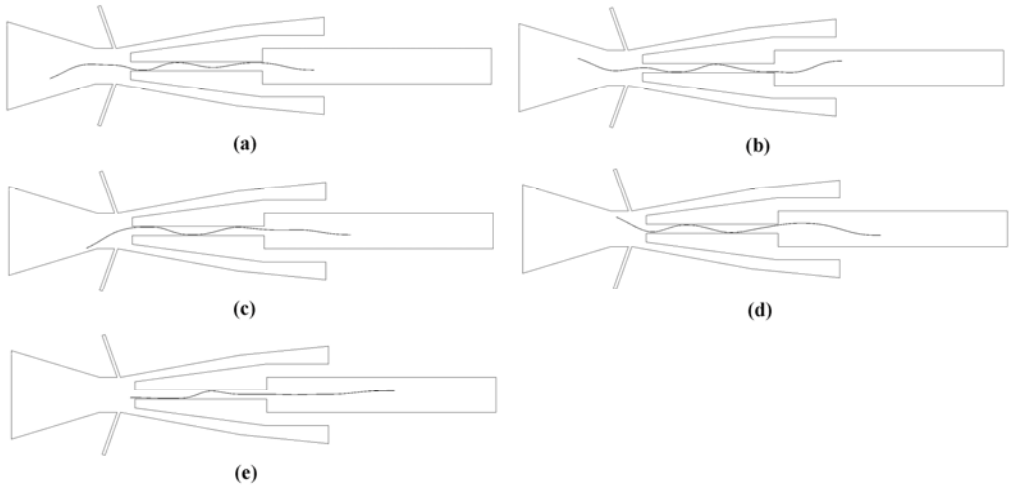

FIGURE 10. Dynamic behavior of the fiber in case D: (a) t=0.00066 s; (b) t=0.00097 s; (c) t=0.00134 s; (d) t=0.00165 s; (e) t=0.00214 s.

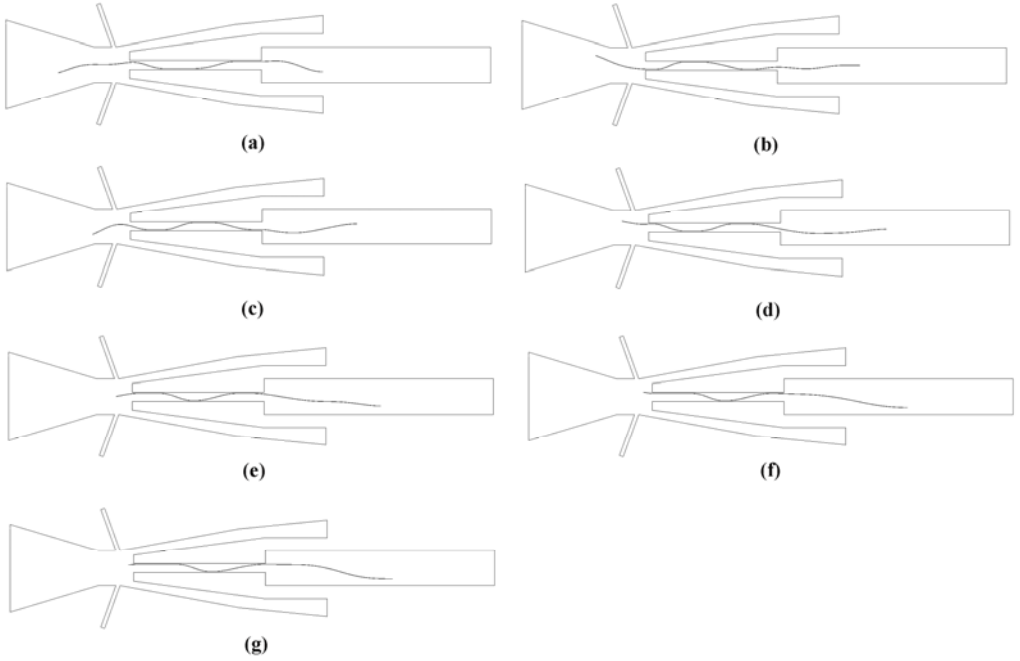

FIGURE 11. Dynamic behavior of the fiber in case E: (a) t=0.00085 s; (b) t=0.00126 s; (c) t=0.0015 s; (d) t=0.00171 s; (e) t=0.00192 s; (f) t=0.00206 s; (g) t=0.00213 s.

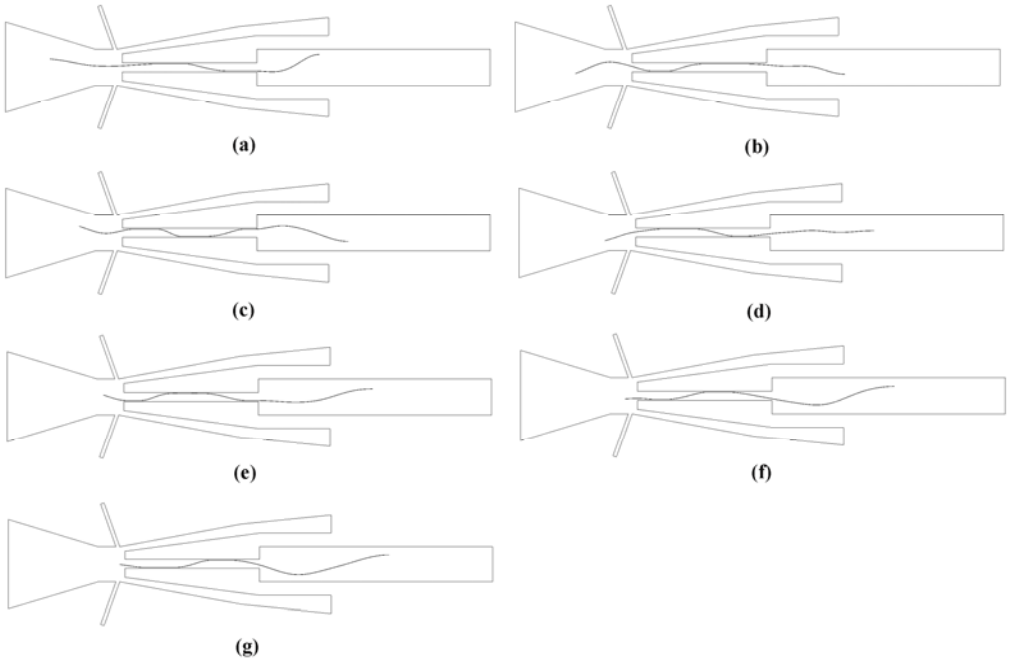

FIGURE 12. Dynamic behavior of the fiber in case F: (a) *t*=0.00068 s; (b) *t*=0.00098 s; (c) *t*=0.00123 s; (d) *t*=0.00147 s; (e) *t*=0.00167 s; (f) *t*=0.00182 s; (g) *t*=0.00196 s.

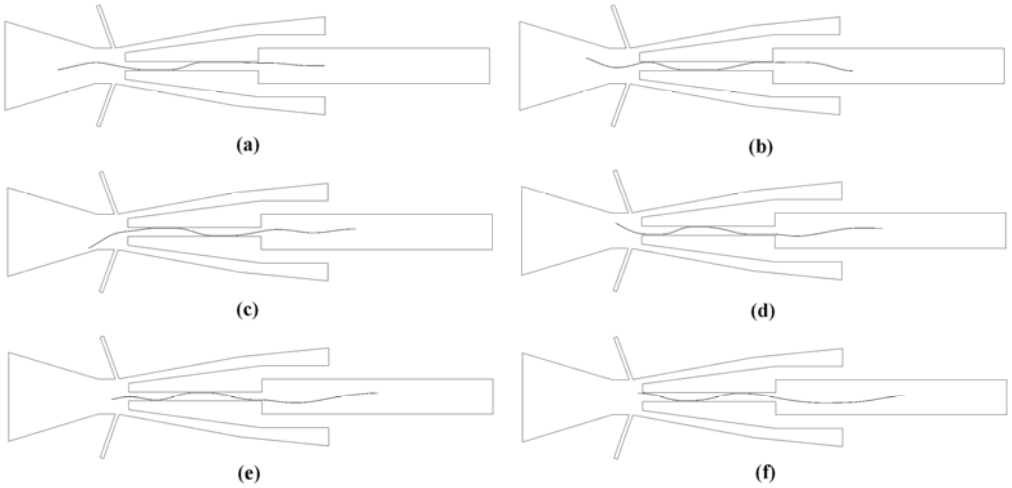

FIGURE 13. Dynamic behavior of the fiber in case G: (a) *t*=0.00085 s; (b) *t*=0.00111 s; (c) *t*=0.00139 s; (d) *t*=0.00164 s; (e) *t*=0.00181 s; (f) *t*=0.00206 s.

According to the simulation results of the dynamic behavior of the fiber, the optimum jet orifice angle for producing vortex spun yarn with the highest tenacity is 70°. Further increase of the jet orifice angle will lead to the decrease of the yarn tenacity.

Effect of the Jet Orifice Diameter

Figure 10 and *Figure 11* illustrate the dynamic behavior of the fiber when the jet orifice diameter is 0.35 mm (Case D) and 0.45 mm (Case E), respectively. In the case when the jet orifice angle is

0.45 mm, the splay degree of the trailing end of the fiber is the lowest. The trailing end of the fiber undergoes three wrapping periods before entering the hollow spindle entirely. Therefore, three twists are inserted into the yarn. During all the three wrapping periods, the rotational amplitude is the smallest of the three cases. In the case when the jet orifice diameter is 0.35 mm, the splay degree of the trailing end of the fiber is similar to the case when the jet orifice diameter is 0.4 mm (case B). The trailing end takes only two wrapping periods to finish the twist insertion process. During the second wrapping period, the rotational amplitude is the largest of the three cases. When the jet orifice diameter is 0.4 mm, three and a half wrapping periods of the trailing end of the fiber take place. During the first wrapping period, the rotational amplitude is similar to that when the jet orifice diameter is 0.35 mm. Based on the simulation results above, the optimum jet orifice diameter is 0.4 mm and a further increase of the jet orifice diameter is not useful.

Effect of the Distance between the Nozzle Inlet and the Hollow Spindle

Figure 12 and *Figure 13* illustrate the dynamic behavior of the fiber when the distance between the nozzle inlet and hollow spindle is 13 mm (Case F) and 13.5 mm (Case G). In the case when the distance between the nozzle inlet and hollow spindle is 13 mm, the trailing end of the fiber undergoes wrappings for three periods before it enters the hollow spindle entirely. The rotational amplitude is the smallest of the three cases during all the three wrapping periods. In the case when the distance between the nozzle inlet and hollow spindle is 13.5 mm, the splay degree is the lowest. It can be seen that the splay degree of the trailing end of the fiber does not show an agreement with the expectation that the splay degree of the fiber increases with increased distance between the nozzle inlet and hollow spindle. In this case, only two and a half wrapping periods of the trailing end of the fiber take place. During the second and the last half wrapping periods, the trailing end of the fiber has the largest rotational amplitude. In the case when the distance between the nozzle inlet and hollow spindle is 14 mm (Case B), the splay degree of the trailing end of the fiber is the highest of the three cases. The trailing end of the fiber takes three and a half periods of the wrapping before completely entering the hollow spindle. This means three and a half twists, which are the most among the three cases, are inserted into the vortex spun yarn. During the first wrapping period, the rotational amplitude is similar to the case when the distance between the nozzle inlet and hollow spindle is 13.5 mm. Based on the numerical analysis above, the optimum distance between the nozzle inlet and the hollow spindle is 14 mm.

CONCLUSIONS

This paper presents a numerical investigation of the dynamic behavior of a cotton fiber and the fiber-airflow interaction inside the vortex spinning nozzle. A two-dimensional fluid-structure interaction (FSI) model combined with the fiber-wall contact is constructed. The effects of three nozzle structure parameters – the jet orifice angle, jet orifice diameter, distance between the nozzle inlet and the hollow spindle, on the dynamic behavior of the fiber, in turn, the yarn structure and tensile property, are studied.

The airflow in the nozzle chamber shows an unsteady vortex structure. Two vortices with momentarily changed sizes are created upstream of the jet orifice outlets. The imbalance of the pressure around the fiber causes the fiber to move and deform. The fiber moves downstream into the hollow spindle with wave shape and is in frequent contact with the internal wall of the hollow spindle. The trailing end of the fiber rotates helically within the nozzle chamber for several periods and to insert twist into the yarn. The simulation results show that the appropriate jet orifice angle for obtaining the best yarn tenacity is 70°. The optimal jet orifice diameter is 0.4 mm. The spun yarn has the highest tenacity when the distance between the nozzle inlet and the hollow spindle is 14 mm.

ACKNOWLEDGEMENTS

This research was funded in part through a grant No. 08JC1400300 by the Key Basic Research Foundation of Shanghai.

REFERENCES

[1] Li, Q., et al., The Dimensional and Mechanical Properties of Wool/Polyester Fabrics Made from Vortex and Ring-Spun Yarns, *Journal of the Textile Institute*, 99(6), 2008, 561 – 568.

[2] Price, C., et al., Relationship of Fiber Properties to Vortex Yarn Quality via Partial Least Squares, *Journal of Engineered Fibers and Fabrics*, 4(4), 2009, 37-46.

[3] Deno, K., Spinning Apparatus with Twisting Guide Surface, *USP* 5528895, 1996.

[4] Oxenham, W., Acar, M., Yu, C., Fiber Motion and Yarn Forming in High Speed Air Flows, National Textile Center *Annual Report* F99-S06, 2000.
[5] Cai, Y., Computer Modeling of Fiber Motion in High-Speed Airflow, *Doctoral dissertation*, NCSU, Raleigh, 2003.
[6] Pei, Z., Yu, C., Study on the Principle of Yarn Formation of Murata Vortex Spinning Using
[7] Lin, J. Z., Wang, C. B., Shen, L. P., The Effect of Fiber Additives on the Turbulent Jets, *International Journal of Nonlinear Sciences and Numerical Simulation*, 4(3), 2003, 227-232.
[8] Ku, X., Lin, J., Fiber Orientation Distributions in Slit Channel Flows with Abrupt Expansion for Fiber Suspensions, *Journal of Hydrodynamics*, 20(6), 2008, 696-705.
[9] Yamamoto, S., Matsuoka, T., Viscosity of Dilute Suspensions of Rodlike Particles: A Numerical Simulation Method, *Journal of Chemical Physics*, 100(4), 1994, 3317-3324.
[10] Skjetne. P., Ross. R. F., Klingenberg, D. J., Simulation of Single Fiber Dynamics, *Journal of Chemical Physics*, 107(6), 1997, 2108-2121.
[11] Kong, L. X., Platfoot, R. A., Computational Two-Phase Air/Fiber Flow Within Transfer Channels of Rotor Spinning Machines, *Textile Research Journal*, 67(4), 1997, 269-278.
[12] Zeng, Y. C., Yu, C. W., Mixed Euler-Lagrange Approach to Modeling Fiber Motion in High Speed Air Flow, *Applied Mathematical Modelling*, 29, 2005, 253-261.
[13] Ortlek, H. G., et al., Effect of Spindle Diameter and Spindle Working Period on the Properties of 100% Viscose MVS Yarns, *Fibres & Textiles in Eastern Europe*, 16(3), 2008, 17-20.
[14] Soe, A. K., et al., Structure and Properties of MVS Yarns in Comparison With Ring Yarns and Open-End Rotor Spun Yarns, *Textile Research Journal*, 74(9), 2004, 819-826.
[15] Ortlek, H. G., Ulku, S., Effect of Some Variables on Properties of 100% Cotton Vortex Spun Yarn, *Textile Research Journal*, 75(6), 2005, 458-461.
[16] Basal, G., Oxenham, W., Effects of Some Process Parameters on the Structure and Properties of Vortex Spun Yarn, *Textile Research Journal*, 76(6), 2006, 492-499.
[17] Guo, H. F., et al., A Numerical and Experimental Study on the Effect of the Cone Angle of the Spindle in Murata Vortex Spinning Machine, *ASME Journal of Fluids Engineering*, 130, 2008, 031106-1-5.
[18] Pei, Z. G., Yu, C. W., Numerical and Experimental Research on the Influence of Parameters on the Tensile Property of Murata Vortex Yarn, *Journal of the Textile Institute*, DOI: 10.1080/00405000903031228.
[19] Bathe, K. J., Finite Element Procedures, Prentice Hall: Upper Saddle River, New Jersey, 1996.
[20] Bathe, K. J., Zhang, H., A Mesh Adaptivity Procedure for CFD and Fluid-Structure Interactions, *Computers and Structures*, 87, 2009, 604-617
[21] Zeng, Y. C., Yu, C. W., Numerical Simulation of the Fiber Motion in the Nozzle of an Air-jet Spinning Machine, *Textile Research Journal*, 74(2), 2004, 117-122.

AUTOHRS' ADDRESSES

Zeguang Pei
Chongwen Yu
Donghua University
College of Textiles
No.2999 North Renmin Road
Shanghai, 201620
CHINA